Chem. Chem. Technol., 2025,
Vol. 19, No. 4, pp. 770–782

Chemical Technology

OPTIMIZATION AND MODELING OF ADSORPTION–DESORPTION SYSTEMS FOR LIQUID-PHASE PROPANE-PROPYLENE PURIFICATION

***Fazil Rahimli*[1,✉], *Nigar Mamedova*[1]**

[1] Department of Petrochemical Technology and Industrial Ecology, Azerbaijan State Oil and Industry University, 34, Azadliq Ave., AZ1010, Baku, Republic of Azerbaijan
✉ *rahimlifazil4@gmail.com*

https://doi.org/10.23939/chcht19.04.770

Abstract. This study investigated the adsorption-desorption performance of three structured adsorbents, 3A-EPG, AZ-500, and SG-731, used in a layered fixed-bed configuration to remove contaminants from a liquid-phase feed mixture composed of 34.2 % propane, 64.5 % propylene, and 1.3 % C4 hydrocarbons. The initial concentrations of impurities were 300 ppm H_2O, 14 ppm RSH, 5 ppm H_2S, and 18 ppm COS. All three adsorbents demonstrated high purification efficiency, reducing impurity concentrations to below 0.1 ppm. Thermodynamic analysis indicated that adsorption efficiency improved with increased pressure and decreased temperature, while higher flow rates marginally reduced performance due to shorter contact time.

Keywords: sulfur removal, molecular sieves, contaminants, separation, sulfur compounds.

1. Introduction

The purification of propane-propylene fractions (PPFs) is a critical step in petrochemical processing, particularly following catalytic cracking operations where hydrocarbon mixtures are often contaminated with undesirable impurities. These impurities, such as water, hydrogen sulfide, mercaptans (RSH), and carbonyl sulfide (COS), must be removed before the stream can be utilized for downstream applications, including polymer-grade propylene production. The presence of these contaminants not only reduces product quality but also poisons catalysts and promotes corrosion in equipment used in polymerization and other refining stages.

Traditionally, chemical scrubbing and drying techniques have been employed for PPF purification. However, these methods tend to be energy-intensive and difficult to integrate into compact systems, prompting a shift toward adsorption-based approaches. Adsorption using porous solids offers a versatile, regenerable, and cost-effective method for the selective removal of trace impurities in both gas and liquid hydrocarbon streams.[1]

Zeolite-based materials have been widely used for moisture and sulfur removal due to their high thermal stability, ion-exchange capacity, and strong affinity for polar molecules.[2, 3] Aluminosilicate adsorbents, such as 3A and 13X, have shown excellent water removal capabilities in hydrocarbon streams. For instance, Seabra *et al.*[4] highlighted the performance of zeolite 13X in achieving deep dehydration of light hydrocarbon mixtures under pressurized conditions. Similarly, Cheng and Wilson[5] demonstrated the robust behavior of AlPO-based materials for selective adsorption of sulfur species under pressure swing conditions, emphasizing their adaptability in regenerable purification systems.

Hybrid adsorbents that combine zeolitic and alumina components, such as AZ-500, are increasingly explored due to their ability to handle multicomponent impurity profiles. These materials exploit both microporous molecular sieving and surface acid-base interactions, enhancing the adsorption of polar contaminants like H_2S and RSH. As Hu *et al.*[6] noted in the context of desulfurization, composite adsorbents with tunable acidity and pore architecture are particularly effective in handling complex sulfur chemistry in hydrocarbon purification. Activated alumina-based materials, such as SG-731, are also widely used in industrial desulfurization units due to their strong affinity for acidic gases and organosulfur compounds. Lei *et al.*[7] reported that alumina adsorbents exhibit enhanced performance for COS and mercaptan removal owing to their Lewis acidity and favorable mesoporous structure, which supports both physisorption and weak chemisorption.

Porous coordination frameworks like metal-organic frameworks (MOFs) and Hydrogen-bonded organic frameworks (HOFs) have been investigated for similar applications, although their thermal and hydrocarbon stability remains a concern under industrial conditions. Su *et al.*[8] and Li *et al.*[9] explored dynamic structural adaptability in PCPs and ultramicroporous HOFs for trace impurity adsorption, but long-term stability in olefin-rich, high-pressure liquid streams remains a major limitation. Likewise, Yang *et al.*[10] and Khraisheh *et al.*[11] proposed ionic liquid-based extractive purification, achieving significant energy savings, but the high viscosity and environmental impact of these solvents hinder industrial scalability. Membrane-based purification methods have also been examined for sulfur and moisture removal in hydrocarbons. However, as Guo and Kanezashi[12] and Xie *et al.*[13] observed, challenges related to membrane fouling, durability under high-pressure liquid-phase conditions, and selective permeability to small polar molecules limit their widespread adoption in PPF purification.

Despite these advancements, several challenges remain. Many adsorption-based methods require further optimization to enhance selectivity and adsorption capacity under industrial conditions. The stability and scalability of MOFs, PCPs, and HOFs in real-world applications are still under investigation, with concerns regarding structural degradation and long-term performance. While ionic liquids show promise in extractive distillation, the high viscosity and potential environmental impact of ILs need to be addressed. Membrane separation technologies, though energy-efficient, often face limitations in selectivity and permeability, making large-scale implementation challenging. Additionally, kinetic and thermodynamic modeling of adsorption – desorption processes remains an area requiring further refinement to improve predictability and process efficiency.

This work offers a fresh look at the purification of propane-propylene, a crucial step in petrochemical processes, utilizing a layered fixed-bed adsorption system. The novelty of this work is its thorough assessment of three industrial adsorbents, 3A-EPG, AZ-500, and SG-731, under real working conditions at an industrial scale. The work offers fresh perspectives on the adsorbents' kinetic and thermodynamic performance for the simultaneous removal of water and sulphur compounds from propane-propylene feed combinations. Notably, by combining extensive, real-time experiments with intricate thermodynamic and kinetic modelling, the research goes beyond conventional laboratory-scale investigations. The results offer significant contributions to the optimization of adsorption-based purification procedures for industrial applications by highlighting important differences from the body of current literature, such as the improved stability and regeneration performance of the chosen adsorbents.

The objective of this study was to analyze the adsorption-desorption characteristics of the adsorbents 3A-EPG, AZ-500, and SG-731 for the treatment of a propane-propylene fraction, specifically targeting the removal of sulfur-containing compounds and water, with an emphasis on evaluating thermodynamic and kinetic parameters to enhance overall purification efficiency. It is hypothesized that, in industrial settings, a layered fixed-bed system employing 3A-EPG, AZ-500, and SG-731 can efficiently eliminate sulfur and moisture impurities from propane-propylene fractions. Each adsorbent is anticipated to target particular pollutants, and chemisorption is confirmed as the primary process using thermodynamic and kinetic models. The study also seeks to show little capacity loss over several cycles and good regeneration efficiency, offering a strong foundation for improving purification procedures at the industrial scale.

2. Experimental

The experimental work in this study was carried out at the Propane-Propylene Fraction Treatment Unit of the Ethylene-Polyethylene Plant located in Azerbaijan. Given the industrial-scale quantities involved 2,970 kg of 3A-EPG, 4,185 kg of AZ-500, and 2,700 kg of SG-731; such testing could not be conducted in a conventional laboratory setting and was therefore performed under real operating conditions at the production facility. The research was conducted over a period of six months, from March 2024 to August 2024, covering the full experimental cycle, including the design and preparation of the adsorption – desorption system, execution of batch experiments, data acquisition, and development of thermodynamic and kinetic models for process optimization.

The study focused on optimizing the adsorption process for treatment of a propane-propylene feed stream using three industrial adsorbents: 3A-EPG, AZ-500, and SG-731. The feed composition included 34.2 mol. % propane, 64.5 mol. % propylene, and 1.3 mol. % C_4S, with contaminant concentrations of H_2O (300 ppm), RSH (14 ppm), H_2S (5 ppm), and COS (18 ppm). Adsorption was performed in the liquid phase at a temperature of 288K and a pressure of 28 atm, with feed rates ranging from 8,000 to 15,000 kg/h. These operating parameters were based on industrial procedures for the purification of propane and propylene, where they guarantee effective mass transfer and ideal adsorption kinetics at high pressure. To prevent thermal degradation of the adsorbents and balance adsorption efficiency, a temperature of 288 K was used. Meanwhile, a pressure of 28 atm increases the adsorption capacity by providing more driving force for the removal of contaminants. In order to maximize process safety and energy usage in

large-scale operations, feed rates were chosen to maintain an effective residence period for impurity removal without resulting in severe pressure reductions or affecting throughput. The molecular weight of the feed mixture was approximately 42.1 g/mol. The adsorbents were layered within the adsorber column in the following order: 3A-EPG (bottom), AZ-500 (middle), and SG-731 (top). The total weights were 2,970 kg for 3A-EPG, 4,185 kg for AZ-500, and 2,700 kg for SG-731. These materials were selected based on their functionality: 3A-EPG for water removal, SG-731 for sulfur compound removal, and AZ-500 as a hybrid for both.

After approximately 120 hours of operation, increased pressure differentials indicated the need for desorption. Regeneration was achieved *via* temperature swing adsorption (TSA) using methane gas (92.5 mol. % CH_4, 4.4 mol. % H_2, with traces of N_2, ethylene, and CO) heated in a furnace. The methane was introduced at 298 K and incrementally heated to 623 K over 7 hours, held at this temperature for 10 hours at a flow rate of 2.1 t/h, and then gradually cooled to 373K. Inside the adsorber, the outlet temperature was maintained at 503 K for 3 hours to enable complete desorption, followed by controlled cooling to 313 K to minimize thermal stress.

Experimental data such as pressure drops, outlet concentrations, and regeneration cycles were used to build a mathematical model for both adsorption and desorption. The model was designed to optimize operating pressure, flow rate, and temperature, as well as to estimate desorption energy and predict the optimal regeneration interval. All experimental data were statistically analyzed to guarantee the results' dependability and reproducibility. The mean values collected from triplicate runs were used to compute breakthrough curves, adsorption capacity, and removal efficiencies; standard deviations were provided to evaluate variability. The equilibrium adsorption data were fitted to regression models, such as Langmuir and pseudo-second-order models, and the residual sum of squares (*RSS*) and R^2 values were used to evaluate the goodness of fit. To make sure that the observed variations were statistically significant, ANOVA tests were also employed to assess the significance of variations in adsorption performance among the adsorbents. Standard software, such as MATLAB, was used to do the analysis, which had a 95 % confidence level.

This integrated experimental and modeling approach aimed to deliver a robust framework for optimizing adsorption-based purification of propane-propylene mixtures under industrial conditions. A propane-propylene feed's contaminant concentrations of H_2O, RSH, H_2S, and COS were continually measured using an online gas chromatograph (Agilent 7890A) fitted with a flame photometric detector and a thermal conductivity detector. To guarantee accurate measurements with a ±1 % precision, the chromatograph was calibrated every day using certified calibration gases with known concentrations (H_2O: 300 ppm, RSH: 14 ppm, H_2S: 5 ppm, and COS: 18 ppm). High-accuracy temperature sensors (RTD PT100) and pressure transducers (Honeywell 26PC) were used to measure temperature and pressure. Before each experimental run, the sensors were calibrated against National Institute of Standards and Technology (NIST)-traceable references[14] to guarantee data dependability. With data being recorded every ten minutes for real-time monitoring and analysis, the calibration checks made sure that all the equipment remained accurate during the experiment.

The removal efficiency for each contaminant was quantified based on inlet and outlet concentrations, which were continuously monitored using online gas chromatography. The removal efficiency RE was calculated using the Eq. (1):

$$RE(\%) = \left(1 - \frac{C_{out}}{C_{in}}\right) \times 100\ \%, \quad (1)$$

where C_{in} is the initial concentration of the contaminant, ppm; and C_{out} is the final concentration measured at breakthrough, ppm. This calculation was applied to each adsorbent under dynamic flow conditions to determine their effectiveness in reducing the contaminant load from the propane-propylene feed.

To accurately model the adsorption behavior of H_2O, H_2S, RSH, and COS on the selected adsorbents, equilibrium adsorption data were analyzed using Langmuir isotherm models. The Langmuir Eq. (2) is expressed as:

$$q_e = \frac{Q_{\max} K_L C_e}{1 + K_L C_e}, \quad (2)$$

where q_e is the equilibrium adsorption capacity, mmol/g; $Q_{\max}$ is the maximum adsorption capacity, K_L is the Langmuir constant, L/mmol, and C_e is the equilibrium concentration of the adsorbate in the gas phase.

To further characterize the adsorption process, kinetic studies were conducted by measuring adsorption uptake at different time intervals and fitting the data to pseudo-first-order and pseudo-second-order models. The adsorption kinetics followed a pseudo-second-order behavior for all contaminants, indicating that chemisorption is the dominant mechanism. The pseudo-second-order Eq. (3) is given by:

$$\frac{t}{q^t} = \frac{1}{k_2 q_e^2} + \frac{t}{q_e}, \quad (3)$$

where q^t is the adsorption capacity at time t, q_e is the equilibrium adsorption capacity, and k_2 is the pseudo-second-order rate constant, g/mmol·min. The superior fit of this model suggests that adsorption is controlled by surface reaction mechanisms rather than simple mass transfer, with active site interactions playing a key role in contaminant uptake.

To explain the adsorption behavior of pollutants on the chosen adsorbents, the Temkin isotherm model was also applied. For systems where adsorption involves interactions between adsorbate molecules, the Temkin model's assumption that the heat of adsorption falls linearly with increasing adsorbent surface coverage is pertinent. The Eq. (4) for the Temkin model is:

$$q_e = \frac{RT}{b}\ln(Ae^{bC_e}), \quad (4)$$

where q_e is the amount of adsorbate adsorbed at equilibrium, mmol/g; C_e is the equilibrium concentration of the adsorbate, mmol/L; A is the Temkin isotherm constant, L/mmol; b is the Temkin constant related to the heat of adsorption, kJ/mol; R is the universal gas constant (8.314 J/mol·K), and T is the temperature, K.

To evaluate the energetic aspects of adsorption, activation energies E_a were determined using Arrhenius plots, where the adsorption rate constant was plotted against the inverse temperature. The Arrhenius Eq. (5) is expressed as:

$$k = Ae^{-E_a/RT}, \quad (5)$$

where k is the adsorption rate constant, A is the pre-exponential factor, E_a is the activation energy, R is the universal gas constant, and T is the temperature, K.

The temperature dependence of adsorption was further analyzed using the van't Hoff Eq. (6):

$$\ln K_L = -\frac{\Delta H}{RT} + C, \quad (6)$$

where ΔH represents the enthalpy change of adsorption. The negative values of ΔH for all adsorbents confirmed that adsorption was exothermic, reinforcing the need for optimized low-temperature conditions for maximum adsorption efficiency.

The desorption energy required for regenerating the adsorbents was calculated by evaluating the total thermal energy input needed to raise the temperature of the adsorbent bed from ambient conditions to the target desorption temperature and maintain it over the required holding time. This includes both sensible heat (required to heat the solid adsorbents and the system) and the heat of desorption (required to release the adsorbed species).

The total energy consumption Q_{total} (in kWh) was determined using the Eq. (7):

$$Q_{total} = Q_{sensible} + Q_{desorption}, \quad (7)$$

where $Q_{sensible} = m \times C_p \times \Delta T$, m is the total mass of adsorbents, kg, C_p is the average specific heat capacity of adsorbents, kJ/kg×K; ΔT is the temperature change from ambient to regeneration temperature, K; $Q_{desorption} = n \times \Delta H_{des}$, n is the number of moles of contaminants desorbed, and ΔH_{des} is the heat of desorption per mole, kJ/mol.

Methane was used as the heating medium, and the flow rate (2.1 t/h) was monitored throughout the process. The total thermal input was further corrected for furnace heat loss and system inefficiencies using an efficiency coefficient (typically 0.85–0.9). The energy was converted from kJ to kWh for industrial comparison. This calculation allowed estimation of the average energy demand per regeneration cycle, which was then normalized to kWh per ton of purified product. The calculated value of approximately 72.4 kWh/ton was used to compare different regeneration profiles and guide optimization of flow rate, ramp time, and holding duration.

3. Results and Discussion

Initial experiments were designed to evaluate the dynamic performance of the adsorbents under continuous feed conditions, with particular focus on breakthrough behavior. Breakthrough curves were obtained by monitoring the concentration of each contaminant at the outlet of the adsorption column as a function of time. These curves are essential in determining the point at which the adsorbent becomes saturated and loses its capacity to remove a particular species from the gas stream. The breakthrough point is typically defined as the time at which the outlet concentration reaches 5 % of the inlet concentration, while the exhaustion point is marked at 95 %. These benchmarks were used to calculate the effective working capacity of each adsorbent under actual operating conditions.

The results clearly indicated that SG-731 outperformed the other two adsorbents in terms of sulfur compound removal, particularly for organosulfur species such as RSH and COS (Table 1). The values presented in Table 1 were derived based on continuous-flow adsorption experiments using online gas chromatography and calculated according to Eq. (1).

Table 1. Contaminant removal efficiencies of selected adsorbents, mol. %

Adsorbent	H_2O removal	RSH removal	H_2S removal	COS removal
3A-EPG	98.2	85.3	91.1	87.4
AZ-500	92.5	89.2	94.7	90.3
SG-731	89.7	95.5	92.8	88.6

Note: material based on breakthrough curve analysis under conditions at 288 K and 28 atm with feed concentrations of 300 ppm H_2O, 14 ppm RSH, 5 ppm H_2S, and 18 ppm COS. Removal efficiency was calculated according to Eq. (1).

The breakthrough for RSH on SG-731 was significantly delayed, with over 95 mol. % of RSH being adsorbed until the adsorbent approached full saturation. This performance is largely attributable to SG-731's high surface area, uniform mesoporous structure, and its alumina-based matrix, which provides active sites capable of forming moderate Lewis acid-base interactions with sulfur-containing functional groups. COS, being a smaller and less polar molecule, typically exhibits weaker interactions with adsorbents; however, SG-731's tailored porosity allowed for effective molecular sieving and moderate physisorption, resulting in delayed COS breakthrough. In contrast, the 3A-EPG adsorbent, composed primarily of clay-based aluminosilicates with microporous characteristics, exhibited remarkable affinity for water. The breakthrough curve for H_2O was extremely flat for an extended duration, indicating that almost all moisture in the feed was removed prior to the onset of saturation. The residual water content in the purified stream consistently remained below 0.05 ppm. This exceptional moisture removal capability is attributed to the strong hydrogen bonding between water molecules and the hydrophilic aluminosilicate framework of 3A-EPG. Furthermore, the small pore size (typically <3 Å) effectively excluded larger hydrocarbon molecules, thus allowing preferential uptake of smaller polar molecules like water.

AZ-500, which integrates both zeolitic micropores and alumina macropores in a hybrid structure, displayed a more balanced adsorption profile. The breakthrough curves for both H_2O and sulfur compounds were intermediate between those observed for 3A-EPG and SG-731. Its structural composition enables both physisorption and moderate chemisorption, making it well-suited for multicomponent adsorption scenarios. For example, the alumina phase contributed to the adsorption of polar molecules like RSH and H_2S, while the zeolite component enhanced selective uptake of moisture through ion-dipole interactions and molecular sieving. This dual functionality rendered AZ-500 particularly promising for complex gas mixtures where both water and sulfur compounds are present.

The equilibrium adsorption analysis demonstrated clear differences in the adsorption capacities of the three tested adsorbents, 3A-EPG, AZ-500, and SG-731, for specific contaminants, as quantified by isotherm modeling at 323 K. Among the isotherm models evaluated, the Langmuir model consistently exhibited the best fit across all adsorbents and contaminants. This was supported by high determination coefficients (R^2 values greater than 0.99) and the lowest *RSS* in comparison to the Freundlich and Sips models. The superior fitting of the Langmuir model indicates that the adsorption process was predominantly monolayer in nature, occurring on well-defined and energetically uniform sites across the surface of each adsorbent.

Maximum adsorption capacities Q_{max} were quantified through nonlinear regression fitting of the experimental isotherm data at 288 K, utilizing the pseudo-second-order model as described in Eq. (2). Table 2 summarizes the Q_{max} of the three adsorbents. It presents a comparative analysis of the adsorption efficiency of each pollutant, emphasizing the material-specific performance. The information can be utilized to direct material selection for targeted pollutant removal in industrial applications since it illustrates the unique characteristics and efficacy of the adsorbents under certain operating conditions.

Table 2. Summary of Q_{max} for different contaminants and adsorbents, mmol/g

Absorbent	H_2O	H_2S	RSH
3A-EPG	5.2	4.8	3.9
AZ-500	4.5	4.8	3.4
SG-731	3.9	3.2	3.9

According to the data analysis, each adsorbent exhibits unique capabilities for particular pollutants. The selective character of 3A-EPG for water removal is demonstrated by its superior performance in H_2O adsorption, which makes it perfect for dehumidification, but its poorer performance for H_2S and RSH. The AZ-500 exhibits adaptability in multicomponent systems with both moisture and sulfur compounds present by providing balanced performance across all pollutants. SG-731's mesoporous shape and acid-base interactions make it quite successful at removing RSH, but its poorer performance for H_2O adsorption suggests that it is more appropriate for removing sulfur compounds than for controlling moisture. The needs of the particular application, such as selective sulfur capture, multicomponent removal, or water dehumidification, determine which adsorbent is best.

In comparison, the adsorption capacities for the other contaminants on these adsorbents were markedly lower, underscoring the specificity of each material for its optimal target. For instance, 3A-EPG showed significantly lower adsorption for sulfur compounds due to the absence of active acid-base sites suitable for binding these less polar molecules (Fig. 1). Likewise, SG-731, though effective for RSH, displayed moderate performance for H_2O and H_2S due to its less hydrophilic nature and broader pore size distribution.

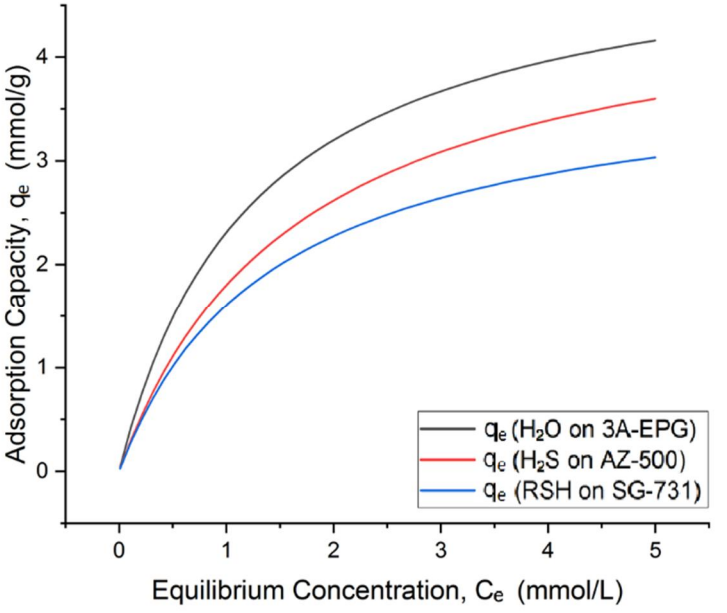

Fig. 1. Langmuir adsorption isotherm

The adsorption kinetics of H_2O, RSH, and H_2S on the adsorbents 3A-EPG, AZ-500, and SG-731 were systematically evaluated under operational conditions of 288 K and 28 atm. Time-dependent adsorption data were collected during batch adsorption experiments and fitted to pseudo-first-order and pseudo-second-order kinetic models to identify the rate-limiting mechanism. The pseudo-second-order model provided a superior fit across all tested adsorbents and contaminants, as confirmed by high regression coefficients (R^2>0.98) and strong agreement between the experimental and calculated equilibrium capacities. These correlations were further supported by low values in residual error and sum of squared errors (*SSE*), validating the reliability of the model fits. The strong conformity to the pseudo-second-order model indicated that chemisorption governed the adsorption process. This suggested that the interaction between the adsorbent surface and the contaminants involved electron sharing or exchange mechanisms, which are characteristic of chemical bonding. The rate-limiting step, therefore, was not mere diffusion or physisorption but the formation of stable surface-adsorbate complexes.

To assess the strength of these interactions, temperature-dependent kinetic measurements were performed at four distinct temperature points (298 K, 313 K, 323 K, and 338 K). Rate constants obtained from these experiments were used to construct Arrhenius plots, from which activation energies (E_a) were calculated based on the linearized form of the Arrhenius Eq. (3). The results are presented in Table 3.

These values quantitatively reflect the relative binding strength of each contaminant on the corresponding adsorbent. The highest activation energy observed for H_2O adsorption on 3A-EPG indicated a strong interaction facilitated by hydrogen bonding and ion-dipole forces. AZ-500 demonstrated intermediate activation energy for H_2S, suggesting effective but moderately strong electrostatic attraction. In contrast, the lower activation energy observed for *RSH* adsorption on SG-731 suggested a mechanism dominated by weaker Van der Waals and π-interactions between the sulfur-containing organics and the alumina surface. These kinetic results were obtained from high-resolution dynamic adsorption data, acquired during real-time breakthrough and batch experiments, ensuring a robust dataset for model validation. The temperature-dependent kinetic profiling confirmed not only the chemisorptive nature of the process but also highlighted the reusability and stability of each adsorbent under cyclic thermal conditions. This insight is essential for predicting performance over extended operation in industrial purification units treating PPFs.

Table 3. E_a for adsorption, kJ/mol

Adsorbent	H_2O	H_2S	RSH
3A-EPG	24.7	21.3	18.9
AZ-500	23.1	22.0	20.5
SG-731	22.3	19.8	17.5

In order to evaluate the adsorption behavior under experimental settings, the Temkin isotherm model was also used to examine the experimental data for contaminant removal (H_2O, RSH, H_2S, and COS). The Temkin model provided a good fit to the data, especially for the adsorption of RSH and H_2S, where notable adsorbate-adsorbate interactions were noted. Table 4 provides a summary of the Temkin model parameters.

Table 4. Temkin isotherm parameters for contaminant adsorption

Contaminant	*A*, L/mmol	*b*, kJ/mol	R^2
H_2O	0.9	2.1	0.96
RSH	0.8	4.5	0.98
H_2S	0.8	5.2	0.99
COS	1.2	3.4	0.91

The adsorption behavior of the pollutants under examination was well-represented by the Temkin model, which also identified unique processes for every component. With moderate adsorption temperatures, which are suggestive of a chemisorption mechanism, the model indicated that considerable adsorbate-adsorbate interactions played a role in the adsorption process for H_2S and RSH. The strong correlation coefficients (R^2>0.98), which validate the model's resilience and its capacity to precisely depict the adsorption of these sulfur-containing chemicals, lend more credence to this. These results demonstrate the importance of surface chemistry in sulfur compound removal, as the adsorbate molecules have a stronger interaction with the adsorbent surface.

The H_2O adsorption data, on the other hand, showed a lower heat of adsorption, indicating a more straightforward adsorption process that is largely fueled by the physical interaction of water molecules with the adsorbent surface rather than by substantial adsorbate-adsorbate effects. This was further supported by the fact that water had a lower Temkin constant than sulfur compounds, suggesting a simpler adsorption mechanism. The Temkin model produced a less accurate result for COS, indicating that pore size effects and molecular sieving were more important in the removal process. This suggests a more physically driven adsorption mechanism in which the pore structure of the adsorbent plays a more important role in the separation of COS molecules than interactions between the adsorbate and the adsorbent.

The Temkin model provided a thorough understanding of the adsorption process in conjunction with the Langmuir isotherm and pseudo-second-order kinetic models. It demonstrated that, although surface coverage is significant, adsorbate-adsorbate interactions, especially for sulfur compounds, are also crucial in determining adsorption efficiency. These findings highlight the need to take into account a variety of models in order to completely represent the intricacy of the adsorption processes involved and show how crucial adsorbent surface characteristics are to maximizing the removal of contaminants in industrial settings.

To evaluate how operational parameters influence adsorption, temperature and pressure studies were conducted. As is characteristic of exothermic adsorption processes, increasing temperature resulted in a noticeable decline in adsorption efficiency across all tested adsorbents. For instance, the adsorption capacity of SG-731 for RSH decreased by approximately 10 % when the temperature was increased from 298 K to 323 K. This temperature sensitivity underscores the thermodynamically exothermic nature of sulfur adsorption, where increased thermal energy reduces the adsorptive forces between the surface and adsorbate, thereby promoting desorption.

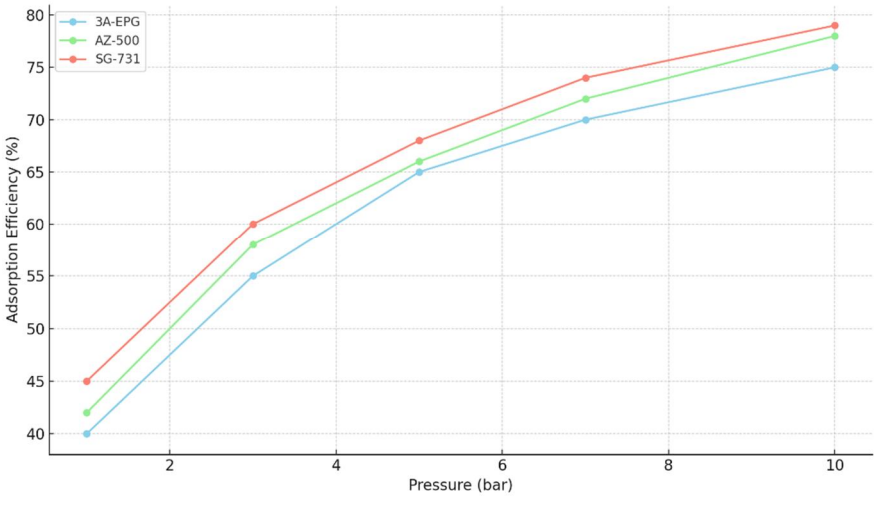

Fig. 2. Pressure influence on adsorption efficiency for different adsorbents

In contrast, pressure had a markedly positive effect on adsorption performance. A pressure-dependent increase in uptake was recorded for each adsorbent and target contaminant. Notably, H_2O adsorption on 3A-EPG improved by 65 % when the pressure was elevated from 1 bar to 10 bar. Similar trends were observed for AZ-500 and SG-731 with respect to H_2S and RSH, respectively (Fig. 2). This enhancement is attributed to the increased driving force for mass transfer under higher pressure conditions, which promotes more frequent and forceful collisions between gas-phase molecules and the adsorbent surface.

Fig. 2 also enables a comparison of each adsorbent's relative efficiency under various pressure conditions. While all materials benefit from higher pressure, some adsorbents (such as SG-731) exhibit superior efficiency, making them more appropriate for applications requiring high-pressure environments. This knowledge is essential for improving industrial processes that require both effective operation under pressure and a high adsorption capacity. However, the benefits of pressure increase diminished beyond 8 bar, where the adsorption curves began to plateau. This suggests that the active sites had approached saturation, and additional pressure provided little marginal gain in adsorption capacity.

Thermodynamic parameters calculated from van't Hoff plots supported the experimental observations. All adsorbents exhibited negative values for enthalpy change ΔH, reaffirming the exothermic nature of the adsorption processes. The strongest enthalpic changes were observed for H_2O on 3A-EPG, which is consistent with its high affinity and large activation energy. Moderate values for H_2S and RSH further validated the chemisorption dominance, though the underlying mechanisms varied in intensity and nature across adsorbents.

The desorption phase of the adsorption cycle is essential for maintaining long-term performance of adsorbents, minimizing operational costs, and ensuring the feasibility of continuous industrial application. A regeneration protocol using methane as the primary heating medium was developed and implemented. Methane gas with a purity of 92.5 mol. %, supplemented by 4.4 mol. % hydrogen and trace amounts of nitrogen, ethylene, and carbon monoxide, was passed through a furnace where it was heated from 298 K to 623 K at a controlled ramping rate of 50 K per hour over 7 hours. This heating profile was chosen to prevent thermal stress and mechanical degradation of the adsorbent materials.

Once the target temperature of 623 K was achieved, the gas flow was maintained at this temperature for 10 hours to ensure full thermal saturation. The preheated gas was then directed through the adsorber columns, progressively raising the internal bed temperature to 503 K. This temperature was sustained for an additional 3 hours to facilitate desorption of all adsorbed species, particularly sulfur-containing compounds such as RSH and COS, which were retained most strongly in the upper SG-731 layer due to its high alumina content and affinity for sulfur compounds. The SG-731's high thermal resistance allowed for effective regeneration without notable degradation in structure. Following the desorption phase, the beds were subjected to a controlled cooling regimen, gradually reducing the temperature to 313 K. This slow and managed cooling was critical for preserving the structural integrity of the adsorbents. Rapid cooling can result in microcracks, pore collapse, or mechanical attrition, all of which significantly reduce the longevity and adsorption capacity of the material.[15–17] No significant degradation or loss in capacity was observed post-cooling, indicating that the protocol successfully mitigated these risks.

The effectiveness of the regeneration process was quantitatively evaluated by assessing the desorption efficiency and adsorbent stability over multiple cycles. Desorption efficiency, defined as the percentage of initially adsorbed contaminants removed during regeneration, exceeded 95 % for all target compounds across all adsorbents. SG-731, despite its high adsorption affinity for sulfur compounds, responded particularly well to the desorption protocol, which is noteworthy considering sulfur species often form stronger, more persistent bonds with alumina-rich surfaces.

The energy consumption associated with the regeneration process was thoroughly evaluated and compared between two widely implemented industrial methods: Pressure Swing Adsorption (PSA) and TSA. The calculations were based on experimentally measured gas flow rates, desorption durations, and temperature profiles. PSA regeneration was performed by reducing the system pressure without significant thermal input, which required an estimated 63 kWh per ton of treated product. This value was derived by integrating the mechanical work done to reduce and re-pressurize the adsorption columns during cyclic operation, using compressor efficiency ($\eta \approx 0.85$), pressure drop (ΔP=25 atm to 5 atm), and volumetric flow rate (~15,000 kg/h of PPF, molecular weight ≈42.1 g/mol). The thermal energy input was calculated using Eq. (6) and resulted in 98 kWh/ton of treated PPF when averaged over total desorbed mass and treatment cycles.

PSA has definite economic advantages over TSA regeneration techniques, according to the cost-benefit analysis, especially for large-scale applications. PSA's energy use leads to a 30 % decrease in energy bills, which directly lowers operating costs. Moreover, TSA systems necessitate a significant investment in high-temperature

thermal equipment, as well as increased maintenance and replacement expenses for heating components. PSA requires lower initial capital investment and incurs fewer maintenance costs over time, making it a more cost-effective option. PSA systems' more straightforward designs also result in lower capital costs and better returns on investment, particularly for sectors with extensive and ongoing operations.[18]

Durability testing was carried out by subjecting the adsorbents to 10 full adsorption-desorption cycles, followed by gravimetric and breakthrough performance testing. AZ-500 retained 92 % of its original adsorption capacity, thanks to its hybrid zeolite-alumina structure, which provides mechanical robustness and thermal resistance. 3A-EPG, with its clay-based aluminosilicate composition, showed slightly reduced durability, maintaining 88.4 % of its original capacity due to some degradation from cyclic thermal exposure. SG-731 had the lowest retention at 85.3 %, most likely due to the sensitivity of its alumina-rich structure to repeated high-temperature desorption of sulfur compounds, especially COS and RSH. These values were derived from repeated batch adsorption runs, comparing initial q_e values to those recorded after each regeneration cycle.

In addition to gas-phase studies, adsorption behavior in the liquid phase was also investigated, reflecting the actual operational conditions in the propane-propylene treatment unit of the ethylene-polyethylene production facility in Azerbaijan. Here, the feedstock was treated at 28 atm and 288 K. Flow rates ranging from 6,000 to 15,000 kg/h were tested to simulate industrial feed delivery. The optimal performance was achieved at a feed rate of 10,000 kg/h, which provided sufficient residence time (estimated residence time ≈45–60 seconds per layer) for mass transfer without causing significant pressure drops or compromising throughput. Higher flow rates (>13,000 kg/h) led to early saturation and reduced removal efficiency due to limited contact time. Conversely, excessively low flow rates (<6,000 kg/h) were impractical for industrial throughput, even though they marginally improved removal efficiency. Therefore, 10,000 kg/h was established as the optimal operating point, striking a balance between kinetics and production requirements.

Pressure variation studies showed that adsorption efficiency increased with pressure up to 6 bar, beyond which no significant improvement was observed. This finding is critical since the vapor pressure of the propane-propylene fraction lies near 8 bar, and pushing operating pressure closer to this value increases energy consumption and equipment load. A setpoint of 6 bar was identified as optimal, balancing adsorption capacity with pump energy demands and safety margins. The final desorption protocol, optimized for methane-based thermal regeneration, included the following parameters:

- flow rate: 2.1 t/h of 92.5 % CH_4;
- ramp-up profile: from 298 K to 623 K over 7 hours at 50 K/h;
- holding time: 3 hours at 503 K;
- cooling: controlled descent to 313 K to prevent thermal shock.

This process ensured >95 % desorption efficiency, particularly in the SG-731 layer, where sulfur species (notably RSH) tend to bind strongly. The stability of outlet temperature and pressure drop across layers confirmed uniform heating and effective regeneration. Additionally, the optimal regeneration gas flow rate and holding temperature were determined to be 2.1 t/h and 503 K, respectively.

Overall, the combination of an optimized propane-propylene feed of 10,000 kg/h, an operating pressure of 28 atm., and a process temperature of 288 K provided the most favorable conditions for achieving efficient and stable purification of propane-propylene fractions. These parameters ensured sufficient residence time, enhanced mass transfer, and minimized energy loss, while remaining within safe operational limits for industrial processing equipment. Among the tested adsorbents, AZ-500 emerged as the most promising material, offering a compelling balance of high removal efficiency for sulfur compounds and water, strong thermal and structural integrity, and outstanding regeneration performance over multiple cycles. Its hybrid alumina-zeolite composition contributed to both selective adsorption and prolonged durability, making it well-suited for continuous processing environments. The integration of this material with tailored desorption protocols, including controlled heating rates, optimal desorption hold time, and energy-efficient regeneration via PSA, further enhanced system performance while reducing operational costs. These findings collectively point to AZ-500's strong applicability in full-scale industrial systems tasked with treating PPFs, particularly prior to downstream polymerization or catalytic conversion processes where impurity removal is critical for product quality and catalyst longevity.

This study provided a comprehensive analysis of PPF purification, emphasizing the advantages and limitations of various adsorbent materials, including zeolites, MOFs, and carbon-based adsorbents. The research focused specifically on three industrial adsorbents: 3A-EPG, AZ-500, and SG-731, engineered for the selective removal of water and sulfur-containing contaminants such as H_2O, RSH, H_2S, and COS from hydrocarbon mixtures obtained from catalytic cracking processes. Compared to MOFs and carbon-based materials, these industrial adsorbents demonstrated

superior thermal stability, mechanical durability, and regeneration performance, reinforcing their suitability for long-term, continuous use in petrochemical treatment systems.

Experimental findings showed that each adsorbent had distinct advantages. 3A-EPG, a microporous clay-based aluminosilicate, exhibited excellent water adsorption capacity due to its strong hydrophilic character and surface polarity. AZ-500, a hybrid composed of zeolitic and alumina phases, demonstrated a balanced ability to remove both water and sulfur compounds, highlighting its value in multicomponent feed purification. SG-731, an alumina-based adsorbent with tailored porosity, showed the highest efficiency in capturing sulfur compounds, especially RSH and COS, due to its surface chemistry and structural design. Langmuir isotherm analysis consistently provided the best fit for all adsorbents, indicating monolayer adsorption behavior, which aligns with previous findings on zeolite and MOF materials.

Previous studies have explored the adsorption properties of porous materials, primarily in the context of gas mixture separations such as olefin-paraffin systems. For example, Jorge *et al.*[19] investigated CuBTC and reported moderate selectivity for propylene based on π-complexation with exposed metal sites – findings that aligned with predictions from Ideal Adsorbed Solution Theory (IAST). Fischer *et al.*[20] enhanced the modeling accuracy for CuBTC by applying density functional theory (DFT), demonstrating improved prediction of adsorption behavior. While these studies focused on molecular separations, the adsorption mechanisms, particularly surface interaction and pore architecture, are directly relevant to purification processes involving the removal of trace impurities. The current study builds on these insights and confirms that readily available industrial adsorbents such as SG-731 and AZ-500 offer high removal efficiencies for H_2O, H_2S, RSH, and COS from PPFs. They surpass many advanced materials in terms of thermal stability, mechanical integrity, and regeneration performance qualities essential for sustainable long-term industrial operation.

MOF systems such as Cu-MOF-74 demonstrated high selectivity for specific components (*e. g.*, propylene), as reported by Abedini *et al.*,[21] but faced limitations in thermal endurance and regenerability. Similarly, Lan *et al.*[22, 23] highlighted the challenges in MOF scalability and structural stability under real-world conditions. In contrast, the current study showed that 3A-EPG and AZ-500 retained adsorption performance across multiple thermal cycles. This observation supported findings by Pérez-Botella *et al.*,[24] who affirmed the industrial resilience of aluminosilicate adsorbents.

Although Martins *et al.*[25] explored simulated moving bed (SMB) configurations using Zeolite 13X for propylene recovery, the complexity of operation limited widespread application. In comparison, this study demonstrated that simpler fixed-bed configurations, layered from 3A-EPG to AZ-500 and SG-731, ensured high-efficiency purification of multicomponent PPF feeds. Computational tools have also been employed in adsorbent screening. Suyetin[26] combined machine learning and molecular dynamics to predict propane-selective MOFs, while Fathi *et al.*[27] modeled adsorption behavior using artificial neural networks (ANNs). While computational insights are valuable for material discovery, this study prioritized experimental validation under realistic operational conditions.

Alternative materials, including carbon molecular sieves (CMS) and ultramicroporous carbon adsorbents, were reported by Ma *et al.*[28] and Yuan *et al.*,[29] respectively, demonstrating excellent kinetic selectivity. However, issues related to mechanical fragility, regeneration, and complex synthesis limited their industrial application. In contrast, SG-731, AZ-500, and 3A-EPG demonstrated stable performance and low degradation under harsh thermal and chemical exposure.

Recent innovations, such as biomimetic MOFs,[30] cation-tuned ZIF frameworks,[31] and materials leveraging C–H···N interactions,[32] introduced novel separation mechanisms, but often lacked sufficient structural resilience and scalability for integration into purification systems. This study's breakthrough experiments confirmed practical advantages of AZ-500 and SG-731, especially in sulfur compound removal. The findings aligned with Xia *et al.*,[33] Zeng *et al.*,[34] and Chen *et al.*,[35] who emphasized the importance of breakthrough testing under continuous flow.

Further support was found in the work of Luna-Triguero *et al.*[36] and Pérez-Botella *et al.*,[24] who highlighted the long-term performance stability of zeolitic materials. This was reflected in the current study's thermodynamic and kinetic evaluations, where Arrhenius and van't Hoff models confirmed chemisorption-dominated behavior and exothermic enthalpy changes, respectively – again consistent with prior computational studies by Kim *et al.*[37] HOFs were another emerging class of adsorbents. Gao *et al.*[38] showed that HOF-16 offered 76 % C_3H_6 uptake and a selectivity of 5.4, but issues with thermal and moisture sensitivity persisted. In contrast, AZ-500 and 3A-EPG retained over 88 % of their capacity after 10 regeneration cycles, validating their resilience under typical plant operating conditions.

While the academic community continues to explore advanced separation media such as MOFs, HOFs, and carbon-based frameworks, this study reaffirmed the

practical value of commercially available adsorbents 3A-EPG, AZ-500, and SG-731 for industrial PPF purification. These materials demonstrated high contaminant removal efficiency, thermal and structural stability over multiple adsorption – desorption cycles, and seamless integration into continuous-flow systems. Their performance under industrially relevant conditions confirms their suitability for catalytic cracking facilities, where PPF streams require reliable pre-treatment to meet the stringent purity standards for downstream polymer production. These findings not only bridge the gap between academic research and real-world application but also highlight the critical role of field-tested materials in delivering sustainable, energy-efficient purification in modern petrochemical operations.

4. Conclusions

This study systematically investigated the adsorption and desorption behavior of three industrial adsorbents: 3A-EPG, AZ-500, and SG-731, for the purification of liquid-phase PPF contaminated with water and sulfur compounds. The adsorption process was carried out under controlled industrial conditions (28 atm, 288 K, feed rates of 8,000–15,000 kg/h). The adsorbents were evaluated based on their contaminant removal efficiency, thermodynamic and kinetic behavior, and regeneration performance.

Equilibrium data were best fitted to the Langmuir isotherm model, indicating monolayer adsorption on homogeneous surfaces. Kinetic modeling showed that all adsorption processes followed pseudo-second-order behavior, consistent with chemisorption mechanisms. Thermodynamic evaluations confirmed the exothermic nature of adsorption: increased temperature reduced adsorption efficiency, consistent with desorption-favored conditions at higher thermal inputs. Among the tested materials, SG-731 demonstrated the highest adsorption capacity for sulfur compounds, achieving removal efficiencies above 99.9 %, particularly for RSH and COS. 3A-EPG exhibited superior water removal performance, reducing moisture levels from 300 ppm to below 0.05 ppm due to its strong hydrophilic properties. AZ-500 presented a balanced profile, effectively adsorbing both moisture and sulfur species, making it a versatile candidate for multicomponent purification tasks.

The Temkin isotherm model supported a chemisorption mechanism by demonstrating that there were substantial adsorbate-adsorbate interactions involved in the adsorption of H_2S and RSH. H2O adsorption, on the other hand, was less affected by these interactions, suggesting a more straightforward procedure. The model performed less well for COS, indicating that pore size effects and molecular sieving were more crucial for its elimination. All things considered, the Temkin model enhanced the Langmuir isotherm by emphasizing the intricacy of adsorption and the role surface interactions play.

Regeneration studies revealed that AZ-500 retained 92 % of its adsorption capacity after 10 full adsorption – desorption cycles, outperforming 3A-EPG (88.4 %) and SG-731 (85.3 %). This durability, along with its dual functionality, supports AZ-500's viability for long-term industrial deployment. Energy consumption analysis further demonstrated that PSA was significantly more energy-efficient than TSA, requiring only 63 kWh/ton of product compared to 98 kWh/ton for TSA. Liquid-phase operation was optimized at a pressure of 28 atm and a feed flow rate of approximately 10,000 kg/h (equivalent to around 0.5 L/min in scaled pilot modules), which provided the best trade-off between contaminant removal, residence time, and industrial throughput.

In spite of encouraging outcomes, a number of the research's limitations require further investigation. Since the slow deterioration and buildup of impurities may affect performance and regeneration efficiency, the adsorbents' long-term mechanical stability and fouling resistance during ongoing industrial usage are still unknown. Furthermore, although they may have an impact on adsorption effectiveness, small variations in temperature or feed composition, which are typical in industrial settings, were not thoroughly examined. The intricacy of multicomponent interactions and heat transfer dynamics in large-scale systems was not adequately captured by the adsorption and desorption models, despite the fact that they fit the experimental data. To guarantee the dependability and effectiveness of adsorbents in industrial applications, future research should concentrate on comprehending fouling mechanisms, optimizing processes using dynamic modeling to account for fluctuating operational conditions, and more thoroughly investigating multicomponent interactions and thermal behavior.

References

[1] Redkina, A.; Konovalova, N.; Kravchenko, N.; Strelko, V. Influence of the Porous Structure of V_2O_5-ZrO_2-SiO_2 Catalyst on Reaction of Propane Dehydrogenation. *Chem. Chem. Technol.* **2022**, *16*, 259–266. https://doi.org/10.23939/chcht16.02.259

[2] Pertko, O.; Voloshyna, Y.; Patrylak, L.; Yakovenko, A. Oxidative CO_2 Dehydrogenation of Butane on Microspherical Zeolite-Containing Composites Based on Ukrainian Kaolin. *Chem. Chem. Technol.* **2025**, *19*, 455–462. https://doi.org/10.23939/chcht19.03.455

[3] Lyubchyk, S. I.; Lyubchyk, S. B.; Lyubchyk, A. I. Characterization of Adsorption Properties Inherent to Zirconia

Dioxide for Different Positions of Yttrium in the ZrO_2–Y_2O_3 Lattice. *Semicond. Phys. Quantum Electron. Optoelectron.* **2022**, *25*, 362–371.
[4] Seabra, R.; Dias, R. O. M.; Regufe, M. J.; Ribeiro, A. M.; Rodrigues, A. E.; Ferreira, A. F. P. Propane and Propylene Separation with Carbon Dioxide at Mild Temperatures by Gas-Phase Simulated Moving Bed in Binderfree Zeolite 13X. *Ind. Eng. Chem. Res.* **2023**, *62*, 12600–12612. https://doi.org/10.1021/acs.iecr.3c01601
[5] Cheng, L. S.; Wilson, S. T. Process for separating propylene from propane (U.S. Patent No. 6,293,999). U.S. Patent and Trademark Office, 2001.
[6] Hu, P.; Hu, J.; Liu, H.; Wang, H.; Zhou, J.; Krishna, R.; Ji, H. Quasi-Orthogonal Configuration of Propylene within a Scalable Metal-Organic Framework Enables its Purification from Quinary Propane Dehydrogenation Byproducts. *ACS Cent. Sci.* **2022**, *8*, 1159–1168. https://doi.org/10.1021/acscentsci.2c00554
[7] Lei, Y.; Yu, Z.; Wei, Z.; Liu, X.; Luo, H.; Chen, Y.; Liang, X.; Kontogeorgis, G.M. Energy-Efficient Separation of Propylene/Propane by Introducing a Tailor-Made Ionic Liquid Solvent. *Fuel* **2022**, *326*, 124930. https://doi.org/10.1016/j.fuel.2022.124930
[8] Su, Y.; Otake, K.; Zheng, J. J.; Wang, P.; Lin, Q.; Kitagawa, S.; Gu, C. Diffusion-Rate Sieving of Propylene and Propane Mixtures in a Cooperatively Dynamic Porous Crystal. *Nat. Commun.* **2024**, *15*, 2898. https://doi.org/10.1038/s41467-024-47268-7
[9] Li, L.; Xiang, F.; Li, Y.; Yang, Y.; Yuan, Z.; Chen, Y.; Yuan, F.; He, L.; Xiang, S.; Chen, B.; Zhang, Z. Optimizing Propylene/Propane Sieving Separation through gate-Pressure Control within a Flexible Organic Framework. *Angew. Chem. Int. Ed.* **2025**, *64*, e202419047. https://doi.org/10.1002/anie.202419047
[10] Yang, L.; Liu, Y.; Zheng, F.; Shen, F.; Liu, B.; Krishna, R.; Zhang, Z.; Yang, Q.; Ren, Q.; Bao, Z. Leveraging Diffusion Kinetics to Reverse Propane/Propylene Adsorption in Zeolitic Imidazolate Framework-8. *ACS Nano* **2024**, *18*, 3614–3626. https://doi.org/10.1021/acsnano.3c11385
[11] Khraisheh, M.; AlMomani, F.; Walker, G. High Purity/Recovery Separation of Propylene from Propyne Using Anion Pillared Metal-Organic Framework: Application of Vacuum Swing Adsorption (VSA). *Energies* **2021**, *14*, 609. https://doi.org/10.3390/en14030609
[12] Guo, M.; Kanezashi, M. Recent Progress in a Membrane-Based Technique for Propylene/Propane Separation. *Membranes* **2021**, *11*, 310. https://doi.org/10.3390/membranes11050310
[13] Xie, F.; Wang, H.; Li, J. Microporous Metal-Organic Frameworks for the Purification of Propylene. *J. Mater. Chem. A* **2023**, *11*, 12425–12433. https://doi.org/10.1039/D2TA09326J
[14] National Institute of Standards and Technology (NIST). Resources: Calibration Procedures. **2025**. https://www.nist.gov/pml/owm/laboratory-metrology/documentary-standards-and-resources/calibration-procedures
[15] Kuznetsov, B. N.; Chesnokov, N. V.; Mikova, N. M.; Zaikovskii, V. I.; Drozdov, V. A.; Savos'kin, M. V.; Yaroshenko, A. M.; Lyubchik, S. B. Texture and Catalytic Properties of Palladium Supported on thermally expanded natural graphite. *React. Kinet. Catal. Lett.* **2003**, *80*, 345–350. https://doi.org/10.1023/B:REAC.0000006144.22936.ac
[16] Kuznetsov, B. N.; Chesnokov, N. V.; Mikova, N. M.; Drozdov, V. A.; Shendrik, T. G.; Lyubchik, S. B.; Fonseca, I. M. Properties of Palladium Catalysts on Carbon Supports Prepared from Chemically Modified and Activated Anthracites. *React. Kinet. Catal. Lett.* **2004**, *83*, 361–367. https://doi.org/10.1023/B:REAC.0000046098.90626.56
[17] Shylo, A.; Doroshkevich, A.; Lyubchyk, A.; Bacherikov, Y.; Balasoiu, M.; Konstantinova, T. Electrophysical Properties of Hydrated Porous Dispersed System Based on Zirconia Nanopowders. *Appl. Nanosci. Switz.* **2020**, *10*, 4395–4402. https://doi.org/10.1007/s13204-020-01471-2
[18] Babak, V. P.; Scherbak, L. M.; Kuts, Y. V.; Zaporozhets, A. O. Information and Measurement Technologies for Solving Problems of Energy Informatics. *CEUR Workshop Proceed.* **2021**, *3039*, 24–31. https://ssrn.com/abstract=3987938
[19] Jorge, M.; Lamia, N.; Rodrigues, A. E. Molecular Simulation of Propane/Propylene Separation on the Metal-Organic Framework CuBTC. *Colloids Surf., A* **2010**, *357*, 27–34. https://doi.org/10.1016/j.colsurfa.2009.08.025
[20] Fischer, M.; Gomes, J. R.; Fröba, M.; Jorge, M. Modeling Adsorption in Metal-Organic Frameworks with Open Metal Sites: Propane/Propylene Separations. *Langmuir.* **2012**, *28*, 8537–8549. https://doi.org/10.1021/la301215y
[21] Abedini, H.; Shariati, A.; Khosravi-Nikou, M. R. Adsorption of Propane and Propylene on M-MOF-74 (M=Cu, Co): Equilibrium and Kinetic Study. *Chem. Eng. Res. Des.* **2020**, *153*, 96–106. https://doi.org/10.1016/j.cherd.2019.10.014
[22] Lan, T.; Li, L.; Chen, Y.; Wang, X.; Yang, J.; Li, J. Opportunities and Critical Factors of Porous Metal-Organic Frameworks for Industrial Light Olefins Separation. *Mater. Chem. Front.* **2020**, *4*, 1954–1984. https://doi.org/10.1039/D0QM00186D
[23] Lan, T.; Yu, B.; Liu, Y.; Ning, D.; Zhi, C.; Chen, Y.; Sun, L. B.; Cui, X.; Li, J.; Li, L. Two-Dimensional Anion-Pillared Metal-Organic Framework for Sieving Separation of Propylene from Propane with Ultrahigh Kinetic Performance. *Inorg. Chem.* **2025**, *64*, 5322–5330. https://doi.org/10.1021/acs.inorgchem.5c00602
[24] Pérez-Botella, E.; Valencia, S.; Rey, F. Zeolites in Adsorption Processes: State of the Art and Future Prospects. *Chem. Rev.* **2022**, *122*, 17647–17695. https://doi.org/10.1021/acs.chemrev.2c00140
[25] Martins, V. F.; Ribeiro, A. M.; Plaza, M. G.; Santos, J. C.; Loureiro, J. M.; Ferreira, A. F.; Rodrigues, A. E. Gas-Phase Simulated Moving Bed: Propane/Propylene Separation on 13X Zeolite. *J. Chromatogr. A* **2015**, *1423*, 136–148. https://doi.org/10.1016/j.chroma.2015.10.038
[26] Suyetin, M. Exploring Propane/Propylene Separation through Molecular Dynamics Simulations of Flexible Metal-Organic Framework Models. **2023**. https://doi.org/10.26434/chemrxiv-2023-cpr0c
[27] Fathi, S.; Rezaei, A.; Mohadesi, M.; Nazari, M. PSO-ANFIS and ANN Modeling of Propane/Propylene Separation Using Cu-BTC Adsorbent. *J. Chem. Pet. Eng.* **2019**, *53*, 191–201. http://doi.org/10.22059/JCHPE.2019.269113.1256
[28] Ma, X.; Williams, S.; Wei, X.; Kniep, J.; Lin, Y. S. Propylene/Propane Mixture Separation Characteristics and Stability of Carbon Molecular Sieve Membranes. *Ind. Eng. Chem. Res.* **2015**, *54*, 9824–9831. https://doi.org/10.1021/acs.iecr.5b02721
[29] Yuan, Y. F.; Wang, Y. S.; Zhang, X. L.; Li, W. C.; Hao, G. P.; Han, L.; Lu, A. H. Wiggling Mesopores Kinetically Amplify the Adsorptive Separation of Propylene/Propane. *Angew. Chem. Int. Ed.* **2021**, *60*, 19063–19067. https://doi.org/10.1002/anie.202106523

[30] Xia, W.; Zhou, Z.; Sheng, L.; Chen, L.; Shen, F.; Zheng, F.; Zhang, Z.; Yang, Q.; Ren, Q.; Bao, Z. Bioinspired Recognition in Metal-Organic Frameworks Enabling Precise Sieving Separation of Fluorinated Propylene and Propane Mixtures. *Nat. Commun.* **2024**, *15*, 8716. https://doi.org/10.1038/s41467-024-53024-8
[31] Huang, X.; Martín-Calvo, A.; Mulder, M. J.; van Acht, S. C.; Gutiérrez-Sevillano, J. J.; García-Navarro, J. C.; Calero, S. Effect of Zeolitic Imidazolate Framework Topology on the Purification of Hydrogen from Coke Oven Gas. *ACS Sustainable Chem. Eng.* **2023**, *11*, 8020–8034. https://doi.org/10.1021/acssuschemeng.2c07006
[32] Wang, S.; Zhang, Y.; Tang, Y.; Wen, Y.; Lv, Z.; Liu, S.; Li, X.; Zhou, X. Propane-Selective Design of Zirconium-Based MOFs for Propylene Purification. *Chem. Eng. Sci.* **2020**, *219*, 115604. https://doi.org/10.1016/j.ces.2020.115604
[33] Xia, W.; Yang, Y.; Sheng, L.; Zhou, Z.; Chen, L.; Zhang, Z.; Zhang, Z.; Yang, Q.; Ren, Q.; Bao, Z. Temperature-Dependent Molecular Sieving of Fluorinated Propane/Propylene Mixtures by a Flexible-Robust Metal-Organic Framework. *Sci. Adv.* **2024**, *10*, eadj6473. https://doi.org/10.1126/sciadv.adj6473
[34] Zeng, H.; Xie, M.; Wang, T.; Wei, R. J.; Xie, X. J.; Zhao, Y.; Lu, W.; Li, D. Orthogonal-Array Dynamic Molecular Sieving of Propylene/Propane Mixtures. *Nature* **2021***, 595*, 542–548. https://doi.org/10.1038/s41586-021-03627-8
[35] Chen, F.; Huang, X.; Guo, K.; Yang, L.; Sun, H.; Xia, W.; Zhang, Z.; Yang, Q.; Yang, Y.; Zhao, D.; Ren, Q.; Bao, Z. Molecular Sieving of Propylene from Propane in Metal-Organic Framework-Derived Ultramicroporous Carbon Adsorbents. *ACS Appl. Mater. Interfaces* **2022**, *14*, 30443–30453. https://doi.org/10.1021/acsami.2c09189
[36] Luna-Triguero, A.; Sławek, A.; Sánchez-de-Armas, R.; Gutiérrez-Sevillano, J. J.; Ania, C. O.; Parra, J. B.; Vicent-Luna, J. M.; Calero, S. π-Complexation for Olefin/Paraffin Separation Using Aluminosilicates. *Chem. Eng. J.* **2020**, *380*, 122482. https://doi.org/10.1016/j.cej.2019.122482
[37] Kim, A. R.; Yoon, T. U.; Kim, E. J.; Yoon, J. W.; Kim, S. Y.; Yoon, J. W.; Hwang, Y. K.; Chang, J. S.; Bae, Y. S. Facile Loading of Cu (I) in MIL-100 (Fe) through Redox-Active Fe (II) Sites and Remarkable Propylene/Propane Separation Performance. *Chem. Eng. J.* **2018**, *331*, 777–784. https://doi.org/10.1016/j.cej.2017.09.016
[38] Gao, J.; Cai, Y.; Qian, X.; Liu, P.; Wu, H.; Zhou, W.; Liu, D. X.; Li, L.; Lin, R. B.; Chen, B. A Microporous Hydrogen-Bonded Organic Framework for the Efficient Capture and Purification of Propylene. *Angew. Chem. Int. Ed.* **2021**, *60*, 20400–20406. https://doi.org/10.1002/anie.202106665

Received: July 03, 2025 / Revised: October 01, 2025 / Accepted: October 06, 2025

ОПТИМІЗАЦІЯ ТА МОДЕЛЮВАННЯ АДСОРБЦІЙНО-ДЕСОРБЦІЙНИХ СИСТЕМ ДЛЯ РІДКОФАЗНОГО ОЧИЩЕННЯ ПРОПАНУ – ПРОПІЛЕНУ

Анотація. *Під час дослідження вивчено адсорбційно-десорбційні властивості трьох структурованих адсорбентів, 3A-EPG, AZ-500 і SG-731, які використовували в конфігурації з шаруватим нерухомим шаром для видалення забруднювачів із рідкої фази сировинної суміші, що складалася з 34,2 % пропану, 64,5 % пропілену і 1,3 % вуглеводнів C_4. Початкові концентрації домішок становили 300 ppm H_2O, 14 ppm RSH, 5 ppm H_2S та 18 ppm COS. Усі три адсорбенти продемонстрували високу ефективність очищення, зменшивши концентрації домішок до рівня нижче ніж 0,1 ppm. Термодинамічний аналіз показав, що ефективність адсорбції зростала зі збільшенням тиску та зниженням температури, тоді як вищі швидкості потоку незначно знижували ефективність через коротший час контакту.*

Ключові слова: *видалення сірки, молекулярні сита, забруднювачі, розділення, сполуки сірки.*